Accepted Manuscript

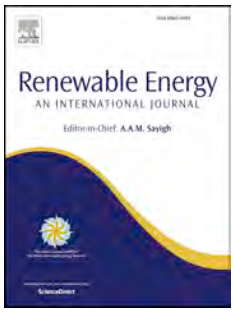

Sustainability indicator for the prevention of potential thermal interferences between groundwater heat pump systems in urban aquifers

Alejandro García-Gil, Sylvia Muela Maya, Eduardo Garrido Schneider, Miguel Mejías Moreno, Enric Vázquez-Suñé, Miguel Ángel Marazuela, Jesús Mateo Lázaro, José Ángel Sánchez-Navarro

PII: S0960-1481(18)31321-1

DOI: https://doi.org/10.1016/j.renene.2018.11.002

Reference: RENE 10765

To appear in: *Renewable Energy*

Received Date: 26 April 2018

Revised Date: 12 October 2018

Accepted Date: 3 November 2018

Please cite this article as: García-Gil A, Muela Maya S, Schneider EG, Mejías Moreno M, Vázquez-Suñé E, Marazuela MiguelÁ, Mateo Lázaro Jesú, Sánchez-Navarro JoséÁ, Sustainability indicator for the prevention of potential thermal interferences between groundwater heat pump systems in urban aquifers, *Renewable Energy* (2018), doi: https://doi.org/10.1016/j.renene.2018.11.002.

Sustainability indicator for the prevention of potential thermal interferences between groundwater heat pump systems in urban aquifers

Alejandro García-Gil[1, 5]*

Sylvia Muela Maya[2]

Eduardo Garrido Schneider[1, 5]

Miguel Mejías Moreno[3]

Enric Vázquez-Suñé[4]

Miguel Ángel Marazuela[4]

Jesús Mateo Lázaro[2]

José Ángel Sánchez-Navarro[2, 5]

[1]Geological Survey of Spain (IGME), C/ Manuel Lasala n° 44, 9° B, 50006 Zaragoza, Spain

[2]Department of Earth Sciences, University of Zaragoza (UZ), c/ Pedro Cerbuna 12, 50009 Zaragoza, Spain

[3]Geological Survey of Spain (IGME) Headquarters, C/ Ríos Rosas 23, 28003 Madrid, Spain

[4]GHS, Institute of Environmental Assessment & Water Research (IDAEA), CSIC, Jordi Girona 18-26, 08034 Barcelona, Spain

[5]Associated Unit in Earth Sciences IGME-UZ

**Corresponding author*

a.garcia@igme.es

Phone: +34 976.55.51.53 Nº fax: +34 976.76.11.06

Abstract

The steady increase of geothermal systems using groundwater is compromising the renewability of the geothermal resources in shallow urban aquifers. To ensure sustainability, scientifically-based criteria are required to prevent potential thermal interferences between geothermal systems. In this work, a management indicator (balanced sustainability index, BSI) applicable to groundwater heat pump systems is defined to assign a quantitative value of sustainability to each system, based on their intrinsic potential to produce thermal interference. The BSI indicator relies on the net heat balance transferred to the terrain throughout the year and the maximum seasonal thermal load associated. To define this indicator, 75 heating-cooling scenarios based in 23 real systems were established to cover all possible different operational conditions. The scenarios were simulated in a standard numerical model, adopted as a reference framework, and thermal impacts were evaluated. Two polynomial regression models were used for the interpolation of thermal impacts, thus allowing the direct calculation of the sustainability indicator developed as a function of heating-cooling ratios and maximum seasonal thermal loads. The BSI indicator could provide authorities and technicians with scientifically-based criteria to establish geothermal monitoring programs, which are critical to maintain the implementation rates and renewability of these systems in the cities.

Keywords: Shallow geothermal energy, GWHP, Urban hydrogeology, indicator, Groundwater, BSI.

1 Introduction

Heating and cooling for buildings accounted for nearly half (544.2 Mtoe) of the final energy consumption in the European Union in 2010 [1]. To fulfill this modern society need, 81% of this energy was generated from combustion processes emitting carbon dioxide (CO_2) [2]. Technologies for heating-cooling using geothermal heat pumps (GHP) could provide such energy requirements by increasing the use of renewable energy sources. GHP installations presented a total installed power of more than 50 GW in 2015 [3], thus presenting a large potential for the mitigation of climate change in this sector [4]. The growing awareness of GHP has resulted in a steady increase of installed capacity worldwide over the last 20 years, with a significant increase of around 10% [5, 6]. This fast spreading of GHP systems all over the world can be explained by their economic and environmental feasibility [7-9], as they are especially economically advantageous when the price of electricity is low [10]. There are two main widespread types of configurations [11]: closed loop and open loop. In close loop or ground-coupled systems, the heat exchanger used to maximize heat transfer with the ground consists in a plastic pipe placed into the ground, either horizontally in a trench or vertically in a borehole. On the other hand, open loop or groundwater heat pump (GWHP) systems pump groundwater or surface water directly as a heat source and circulate it through heat exchangers placed in the surface, finally discharging it into another well or into the same water reservoir [4, 12]. GWHP systems are the oldest type of GHP and were the most widely used until the 90s, when their popularity dropped as environmental regulations raised to prevent aquifer and surface water contamination [13]. Nevertheless, 20 years later, GWHP systems are becoming more common as worldwide governments are cutting back on low-carbon heat sources in favor of renewable heat initiatives. The substantial improvements in energy efficiency and

77 significant reductions in CO_2 emissions experienced in the last years have posed GWHP
78 systems as one of the most powerful systems of geothermal direct use world-wide and they
79 represent a booming sector in geothermal development [6, 14]. The technical potential of
80 GWHP systems for heating and cooling buildings is still large [15] but, to reach their full
81 capability, it is necessary to address different challenges related to regulatory barriers [2,
82 16] and sustainability of the systems related to thermal interference between systems in
83 densely populated urban areas, among others [17]. The management of shallow geothermal
84 resources is a critical point to maintain the implementation rates of these systems in the
85 cities and to ensure, at the same time, their renewability.

86 Although shallow ground is considered as a large energy reservoir, geothermal energy
87 availability in urban areas is limited and overexploitation of the ground is becoming a
88 major concern for authorities [18-20]. The increase in the number of GWHP systems and
89 the increase of thermal interferences between these systems enforces the need for new
90 criteria to develop subsurface energy policies that allow to plan their spatial distribution
91 and to limit their operation regimes. To obtain these sustainability criteria, different
92 approaches have been proposed, beginning with simple rules or threshold values that
93 appear to be empirically defined rather than scientifically evaluated. These first approaches
94 resulted in inconsistent regulative frameworks [16, 21, 22] and have led to failure due to the
95 inability of decision-makers to see the *big picture* and to understand the complexity in an
96 urban environment. This complexity derives from the heterogeneity of hydraulic and
97 thermal parameters in the terrain beneath the cities and, most importantly, from the
98 numerous different flow and heat-transport processes occurring in the urban subsurface,
99 namely surface temperature oscillation throughout the year [23], subsurface building

structures [24, 25], sewage systems [26] or river-aquifer interaction [27], among others. Modifications of the thermal regime of urban aquifers are potentially affecting GWHP systems performance [17]. These potential efficiency changes need to be evaluated with a numerical approach when the grade of complexity involved cannot be handled by simple analytical models [22]. Therefore, a decision-support tool based on numerical modeling for the management of shallow geothermal resources is the most recognized approach [28-32]. Moreover, numerical models at city scale have successfully reproduced the evolution of heat plumes and thermal interferences in urban environments, including complex transient boundary conditions such as real shallow geothermal exploitation regimes [27, 33, 34].

In addition to numerical models, different management criteria have been developed to understand the *big picture* of the resources managed [33]. Concepts such as *present thermal state* compared to *potential natural state* [35] has improved the definition of the thermal impacts from a transient point of view and by considering the thermal memory effect of aquifers. The definition of a relaxation factor [36] allowed to partially improve the temporal allocation of resources by reserving a fraction for future stakeholders. However, a major problem with the application of such management concepts is that they require advanced numerical models that, in turn, demand high resolution monitoring networks for their calibration and validation, and these networks are not always available. Nevertheless, if unsustainable GWPS systems are identified, decision-makers should have facilities to perform a risk assessment of potential thermal interferences affecting the sustainability of managed installations. Furthermore, managers should have a scientifically-based criteria to measure or refine geothermal monitoring networks or to intensify surveillance actuations to focus the efforts towards unsustainable systems.

The main purpose of this study is to develop a management indicator applicable to GWHP systems in a way such that each system could have a quantitative value of sustainability assigned in terms of its intrinsic potential to produce thermal interference. To do this, the theoretical thermal impact generated by GWHP in a standard aquifer of reference calculated by means of numerical modelling was evaluated in 75 heating-cooling scenarios representative of plausible seasonal energy loads. For each of these scenarios, the numerical model gave a thermal impact associated. From a management perspective, the magnitude of these calculated thermal impacts was considered to be proportional to the sustainability of each GWHP system operation scenario considered and, thus, was used directly as a new indicator named BSI. The BSI indicators calculated for 75 heating-cooling scenarios by means of numerical modelling were used to build two simple mathematical models obtaining two polynomial regression models which allowed to relate the BSI to seasonal energy loads. This allows city managers to calculate a sustainable indicator in a simple way directly from a polynomial expression. In conclusion, the BSI indicator appears as a useful decision making tool in the governance of shallow geothermal energy resources in urban areas. The relationship between the net energy transferred to the aquifer and the thermal impact caused is quantified and adopted as an indicator for GWHP systems. The indicator is not expected to predict real thermal impacts of GWHPs but to reflect the degree of sustainability obtained from simple operation parameters of the installations.

2 Methodology

2.1 Definition of the BSI indicator

Heating and cooling demand of buildings vary throughout the year [37]. Although this demand is highly variable depending on the dimensions of the building and its uses, in the

majority of the cases (except in the equator), seasonality exists, thus conditioning the thermal demand of buildings. Therefore, GWHP systems operate with different reversible thermal loads for heating and cooling thorough the year [38]. This feature involves that GWHPs produce heat dissipation during the hot season using the aquifer as a heat sink, and heat absorption during the cold season using the aquifer as a heat source [39]. In this work, it is assumed that the dissipation and absorption periods are 6 months each. According to Chiasson [40], the energy transferred into the aquifer in the cold and hot seasons are referred here as heating load ($E_{Heating}$) and cooling load ($E_{Cooling}$), respectively. The heat net balance throughout a year can be expressed as the ratio of heating and cooling loads ($HC\ Ratio$), defined as:

$$\begin{cases} HC\ Ratio = 1 - \left(\frac{Log_{10}(E_{Cooling})}{Log_{10}(E_{Heating})}\right), E_{Cooling} \geq E_{Heating} \\ HC\ Ratio = 1 - \left(\frac{Log_{10}(E_{Heating})}{Log_{10}(E_{Cooling})}\right), E_{Cooling} < E_{Heating} \end{cases} \quad (1)$$

where $E_{Heating} \geq 1$ and $E_{Cooling} \geq 1$ to ensure division by zero is avoided since logarithms are involved in the definition. This dimensionless ratio is equal to zero when the GWHP system is completely balanced. The logarithmic scale of the thermal loads is justified by the fact that thermal loads present high variability through different orders of magnitude (4 orders of magnitude in this work). The more balanced the thermal load of the GWHP system into the aquifer is, the more sustainable this installation will be (this concept will be proved throughout this work). Table I shows the HC ratio calculated for 23 real GWHP systems studied in previous works [41, 42]. The HC ratio is dimensionless, thus different installations with different thermal loads but same proportion between seasonal loads would present the same ratio. If the maximum seasonal thermal load were considered

167 (Table I) for a given HC ratio, a complete operation scenario would be defined in order to
168 calculate the plausible thermal impact this GWHP system would produce.

169

Groundwater heat pump system	Heating load [MWh]	Cooling load [MWh]	Maximum seasonal thermal load [MWh]	Heating-cooling ratio [-]	BSI simulated [K]	BSI calculated [K]	Error [%]
G-1	4.07E+03	9.34E-01	4.07E+03	0.276	11.276	11.452	1.563
G-2	3.25E+03	8.47E+02	3.25E+03	0.045	6.656	6.659	0.038
G-3	1.92E+03	1.15E+01	1.92E+03	0.173	5.297	5.296	0.011
G-4	1.69E+03	1.97E+02	1.69E+03	0.073	4.132	4.135	0.071
G-5	1.48E+03	1.21E+01	1.48E+03	0.164	4.070	4.068	0.052
G-6	1.71E+03	5.10E+02	1.71E+03	0.041	3.313	3.314	0.033
G-7	9.20E+02	2.11E+01	9.20E+02	0.131	2.489	2.488	0.026
G-8	7.90E+02	1.63E+02	7.90E+02	0.055	1.738	1.738	0.026
G-9	9.52E+02	3.67E+02	9.52E+02	0.033	1.621	1.622	0.021
G-10	8.76E+02	3.49E+02	8.76E+02	0.032	1.460	1.460	0.011
G-11	3.85E+02	0.00E+00	3.85E+02	1.000	1.067	1.051	1.468
G-12	3.46E+02	6.10E+01	3.46E+02	0.062	0.790	0.790	0.011
G-13	1.79E+02	3.79E+01	1.79E+02	0.057	0.390	0.391	0.259
G-14	1.28E+02	4.67E+00	1.28E+02	0.123	0.343	0.344	0.198
G-15	1.09E+02	0.00E+00	1.09E+02	1.000	0.301	0.299	0.553
G-16	3.75E+02	3.02E+02	3.75E+02	0.008	0.201	0.201	0.299
G-17	5.71E+01	0.00E+00	5.71E+01	1.000	0.158	0.157	0.683
G-18	4.39E+01	2.30E-02	4.39E+01	0.293	0.122	0.120	1.438
G-19	1.04E+01	1.43E+01	1.43E+01	0.013	0.011	0.010	7.898
G-20	9.93E+01	1.18E+02	1.18E+02	0.006	0.051	0.052	0.739
G-21	5.16E+01	8.06E+01	8.06E+01	0.017	0.080	0.081	1.674
G-22	4.73E+02	5.35E+02	5.35E+02	0.004	0.171	0.171	0.066
G-23	0.00E+00	6.18E+02	6.18E+02	1.000	1.712	1.673	2.283

170

171 **Table I.** Thermal loads of the 23 GWHP system studied [32] and the parameters required to
172 calculate BSI index. Absolute errors obtained from validation process is also included.

173

174 In this work, a standard model of reference (synthetic numerical model) was defined in
175 order to estimate a thermal impact produced by a GWHP working at a given theoretical
176 operation scenario. The thermal impact produced by each theoretical operation scenario
177 was related to an index value defined as *Balanced Sustainable Index* (BSI). To establish
178 this relationship, multiple regression analysis was performed using MATLAB as well as its
179 Curve Fitting Toolbox [43]. The thermal impact calculated by the standard numerical
180 model or BSI was considered as the independent variable for a given scenario. This

scenario could be defined by 2 dependent variables; (1) the HC ratio (equation 1) and (2) the maximum seasonal thermal load (see Table I). Using multiple regression analysis, a polynomial regression model [44] was obtained to predict BSI as a function of the HC ratio and the maximum seasonal thermal load of the GWHP system. This mathematical model allows to obtain BSI without performing any numerical modelling.

The BSI of a GWHP system represents the thermal impact of a given operational scenario in a standard model considered as a reference framework. The objective of this index is not to predict the real thermal impact of such scenario since a hydrogeological characterization would be necessary. Instead, this index aims to provide a quantitative value proportional to a potential thermal impact produced in a theoretical standardized model. This approach would allow to compare any GWHP system worldwide in a simple way. The following subsections will describe the standard synthetic model constructed and the operational scenarios considered.

2.2 Standard numerical model of reference

A numerical model using finite element code FEFLOW [45], which allows to simulate the conductive and advective heat transport in porous media, was constructed. The two-dimensional (2D) model represented a 3000 m x 1000 m domain (Fig. 1) dimensioned to provide a simulation period of 10 years without border effects. The modeled domain was discretized into an unstructured finite element mesh with 141624 nodes and 71173 triangular elements. The injection well of a GWHP system was implemented by imposing a prescribed flux boundary condition of constant 8 $L \cdot s^{-1}$ inflow (mean injection rate from the 23 real GWHP systems studied) to a node located 500 m away from the up-gradient boundary of the model domain. Fixed head or Dirichlet boundary conditions were adopted

204 to the left and the right model boundaries to represent a regional hydraulic gradient of 1.3E-
205 03. The upper and lower boundaries represent a flow line and Neumann boundary condition
206 with null flux. Steady state was assumed for groundwater flow. A transmissivity of 1500
207 $m^2 \cdot day^{-1}$ were considered, resulting in an averaged Darcy velocity of 0.2 $m \cdot day^{-1}$ for the
208 regional flow. Longitudinal and transversal dispersivities considered were 5 and 0.5 m,
209 respectively, and were assumed to be constant through the domain. A dynamic porosity of
210 0.3 and an aquifer thickness of 10 m were considered. Thermal properties for the whole
211 domain were assumed to be homogeneous. Volumetric heat capacity of water and solid was
212 4.18E6 and 2.52E6 $J \cdot m^3 \cdot K^{-1}$, respectively, and the thermal conductivity adopted for water
213 and solid was 0.65 and 3 $W \cdot m^{-1} \cdot K^{-1}$, respectively. A uniform initial temperature of 0 K was
214 assigned to the whole domain representing the undisturbed aquifer temperature. A fixed
215 temperature of 0 K was prescribed in nodes of the upgradient boundary condition, and a
216 prescribed transient temperature for the injection well was adopted in the node where
217 prescribed flux was imposed. The prescribed temperatures in the inflow node were updated
218 at each time step according to a time function depending on the GWHP system operational
219 scenario considered (scenarios are described in section 2.3). An automatic time-step control
220 with a maximum time-step size of 1 day was used to perform a 10 year simulation period.

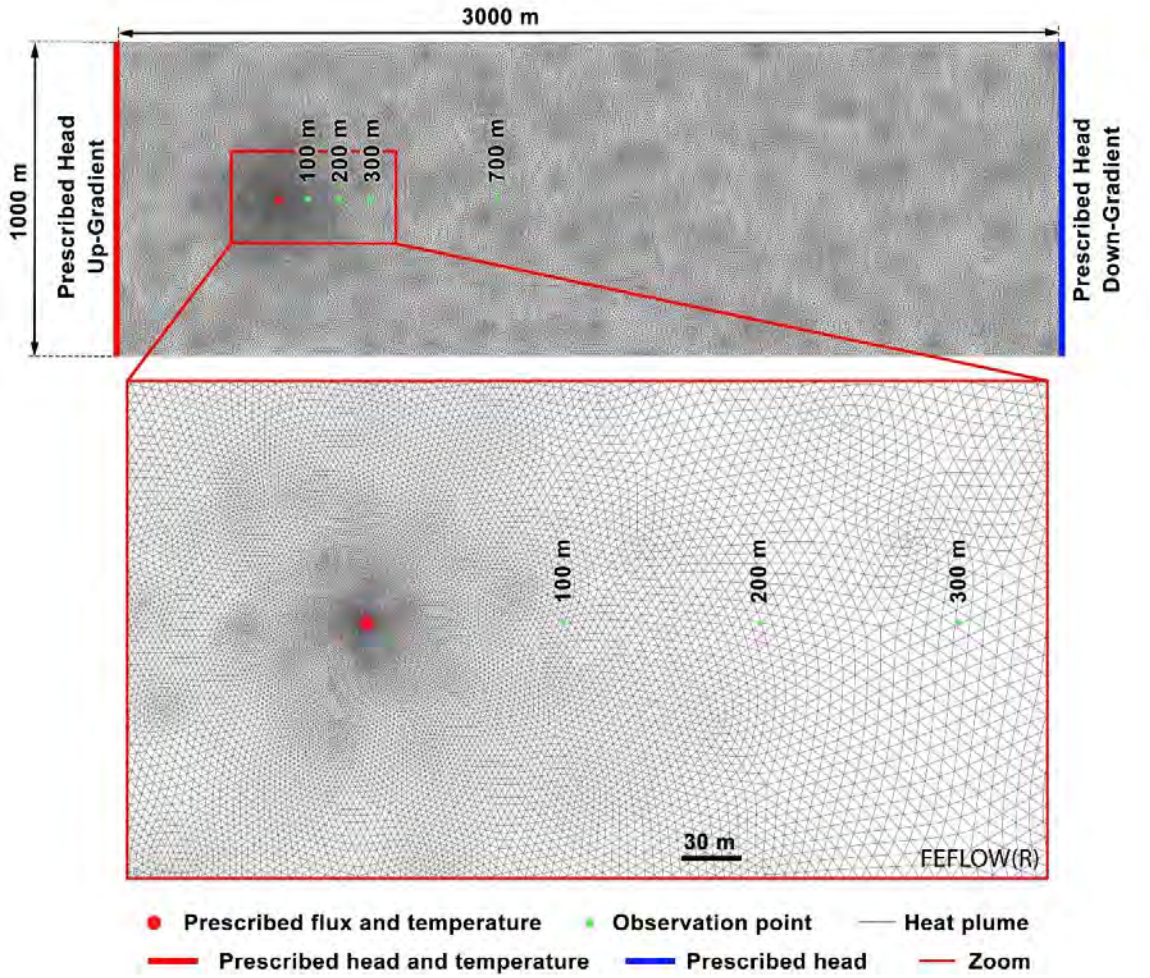

221

222 **Fig. 1.** Figure 1. 2D finite element mesh and boundary conditions used in the standard
223 numerical model used for the definition of the BSI index.

224

225 *2.3 Heating-cooling scenarios*

226 The thermal loads of 23 real GWHP considered in this work (Table I) and the theoretical
227 scenarios used to cover possible thermal loads are shown in Fig. 2. The scenarios combine
228 thermal loads of 8.78, 40.77, 189.24, 878.41 and 4077.19 MWh, and HC ratios of ±1.00,
229 ±0.75. ±0.50, ±0.25, ±0.10, ±0.05, ±0.02 and 0, with negative values representing scenarios

where heating load is greater than cooling and vice versa. Each scenario is divided in two operation periods: the first 6-months period is assumed to transfer a heating load to the aquifer and the following 6-month period considers that a cooling load is transferred to it. This schedule, defined over a year, is extrapolated over 10 years, which is the period required to reach a steady state regime for heat transport at distances greater than 600 m from the injection well. Closer distances respond in a yearly fashion to the seasonal thermal loads imposed. A total of 75 scenarios (see Fig. 2) were simulated by means of the standard numerical model described above to evaluate the standardized thermal impact derived from such scenarios. After the scenario simulations, the thermal impacts generated were considered as the stationary temperature rise after 10 years of exploitation at 700 m from the injection point. The justification of this approach will be discussed in section 3.

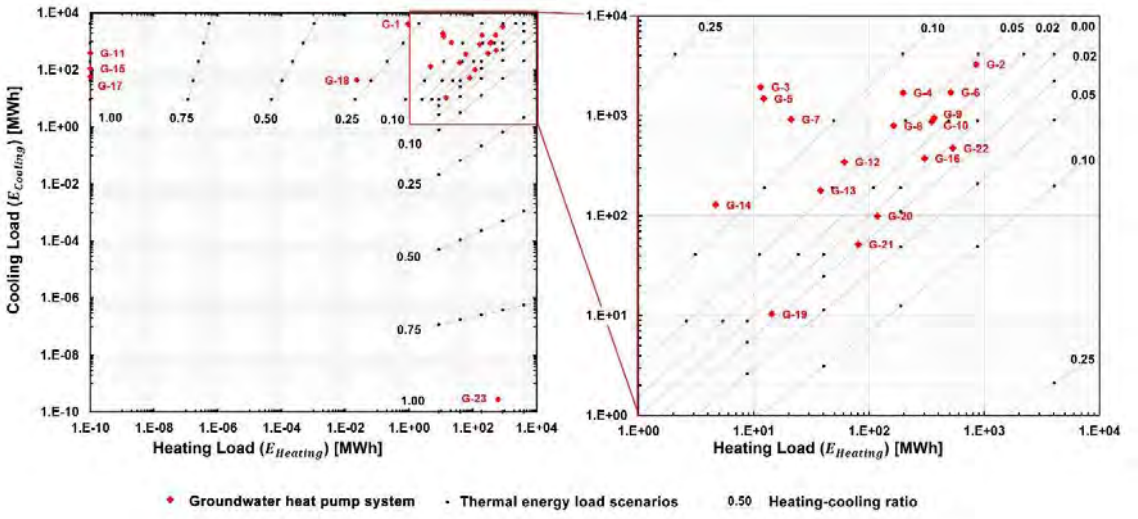

Fig. 2. Thermal energy loads of 23 groundwater heat pump systems from Zaragoza City [32]. Theoretical thermal energy load scenarios simulated for different heating-cooling ratios are also shown.

246 *2.4 Validation of BSI indicator*

247 Polynomial regression models derived from numerical modelling results obtained from the
248 75 heating-cooling scenarios were validated against 23 real GWHPs thermal loads. First,
249 BSI of real GWHP systems was calculated using polynomial regression models derived
250 from the real HC ratios and the maximum seasonal thermal loads of these systems (Table
251 I). Then, BSI of the real GWHP systems were obtained from multiple simulations using the
252 standard numerical model as a reference framework. Differences between calculated and
253 simulated BSI values were evaluated as absolute percentage error.

254 *2.5 BSI indicator calculation of a GWHP system*

255 To calculate the BSI indicator, first the HC ratio [-] (equation 1) of the considered GWHP
256 system needs to be calculated. GWHP systems operating in the 0.00 to 0.10 HC ratio range
257 will consider polynomial regression model 1 and those operating in a HC ratio larger than
258 0.10 will be using polynomial regression model 2 (provided in section 3.2). Polynomial
259 regression models will require, in addition to the HC ratio, the maximum seasonal energy
260 load [MWh]. Once the polynomial regression model is chosen, these two variables allow
261 obtaining the BSI indicator automatically in a simple way. A sample spreadsheet is
262 available as Supplementary Data (S1).

263 **3 Results and discussion**

264 *3.1 Results from the simulation of the defined heating-cooling scenarios*

265 The spatial distribution of thermal impacts is shown in Fig. 3. Spatial distribution of
266 thermal impacts show important damping (exponential decrease) with distance from the
267 injection point and parallel to regional groundwater flow. This occurs independently of the
268 HC ratio. At a certain distance from the injection point, the thermal impact decay is

constant down to zero. This distance can be termed as *damping distance* and is marked on Fig. 3. The thermal impact achieved in this constant zone is closely related to the HC ratio, becoming zero when the heating load is the same as the cooling load. This effect is also appreciated on the heat plume areas, where they are drastically reduced down to a zero value HC ratio. Furthermore, the reduction of the thermal impact extension over space is very sensible to the HC ratio. From ±0.10 to ±1, this reduction is almost negligible and vice versa. This figure also shows that an increase in the maximum seasonal energy load increases heat plumes more effectively in the zero HC ratio scenarios. In addition, heat plumes produced in scenarios with the same absolute ratio generate very similar spatial thermal impacts but with the opposite sign. Differences arise from the fact that the initial heat pulse is for heating by definition.

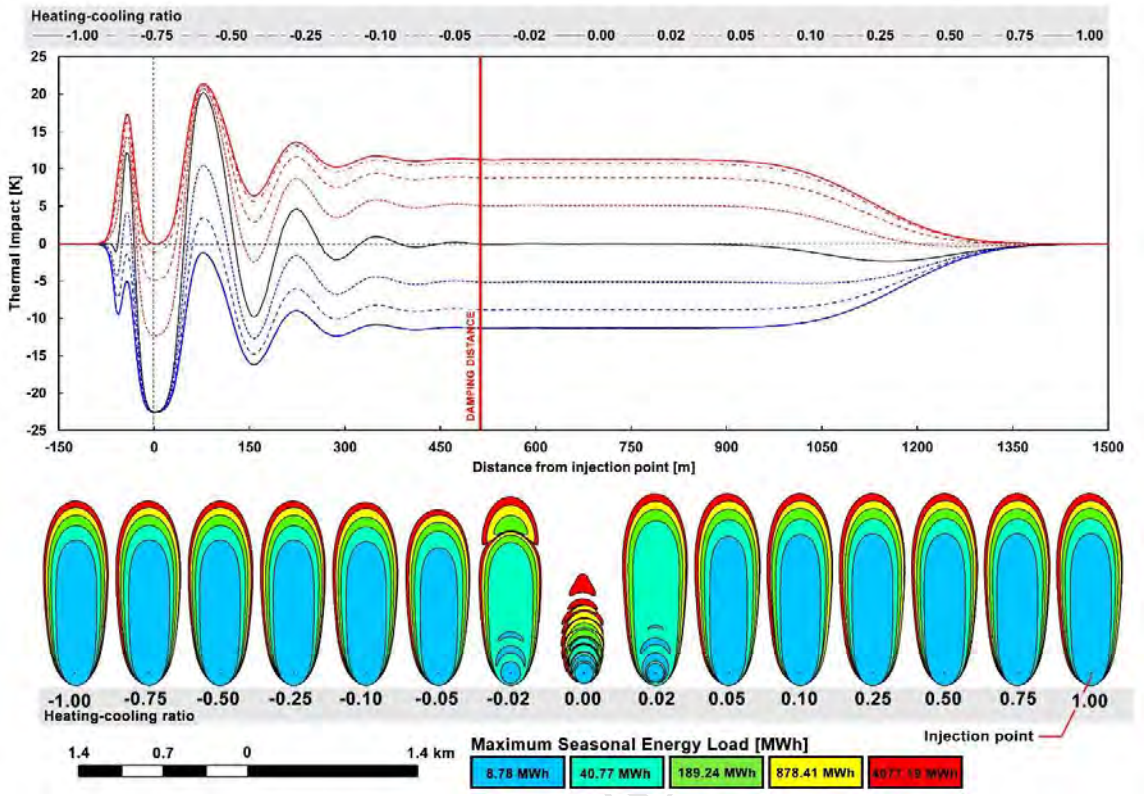

Fig. 3. Spatial distribution of thermal impacts calculated from the simulation of the 75 heating-cooling scenarios after 10 years of simulation. In the top of the figure, the relative thermal impact is represented against distance in the *x* direction from the injection point parallel to regional groundwater flow. The relative thermal impact is shown for different heating-cooling ratios and a maximum seasonal energy load of 4077.19 MWh. In the bottom, the heat plumes extension for a ±0.01 K increase for the different maximum seasonal energy loads is shown. Negative values of the heating-cooling represent heating loads greater than cooling, and vice versa.

The temporal distribution of thermal impacts at 100, 200, 300 and 700 m from the injection point and the 878.4 MWh maximum seasonal energy load are provided in Fig. 4. This

figure shows that, independently of the HC ratio, the thermal impact derived from seasonal schedule of operation produces a cyclic oscillation of thermal impacts downgradient of the injection point. The amplitude depends clearly on the distance at which the thermal impact is evaluated, showing a clear damping of the oscillation amplitude of the thermograms with distance. Nevertheless, the wavelength is the same for all distances where oscillation is observed but oscillations at different distances present a phase difference (retardation). At a certain distance from the injection point, termed here as damping distance, the oscillation of the thermal impact disappears (Fig. 3) and a non-oscillatory impact is produced. At points beyond the damping distance, the thermal impact rises steadily until reaching a stable thermal impact. Moreover, this stable thermal impact corresponds to the origin axis of oscillation at all distances for a given HC ratio. When the cooling loads are greater than the heating ones (Fig. 4A), the non-oscillatory thermal impact is positive, when the cooling loads are the same as the heating loads, the non-oscillatory thermal impact is zero (Fig. 4B) and, finally, when the cooling loads are lower than the heating loads, the non-oscillatory thermal impact is negative. The relationship between non-oscillatory thermal impacts and HC ratios is shown in Fig. 4D. Symmetry of the non-oscillatory thermal impacts should be noted: if the HC ratio sign is inverted, the non-oscillatory thermal impact will have the same magnitude but with the opposite sign. In consequence, the absolute values of non-oscillatory thermal impacts will be considered hereafter in the discussion. Considering all these facts, it is possible to define the *non-oscillatory thermal impact* as the thermal impact produced beyond the damping distance representative of the thermal imbalance of the GWHP system. Therefore, the non-oscillatory thermal impact derived from a given heating-cooling scenario is a possible approach to describe the sustainability of a GWHP system.

318

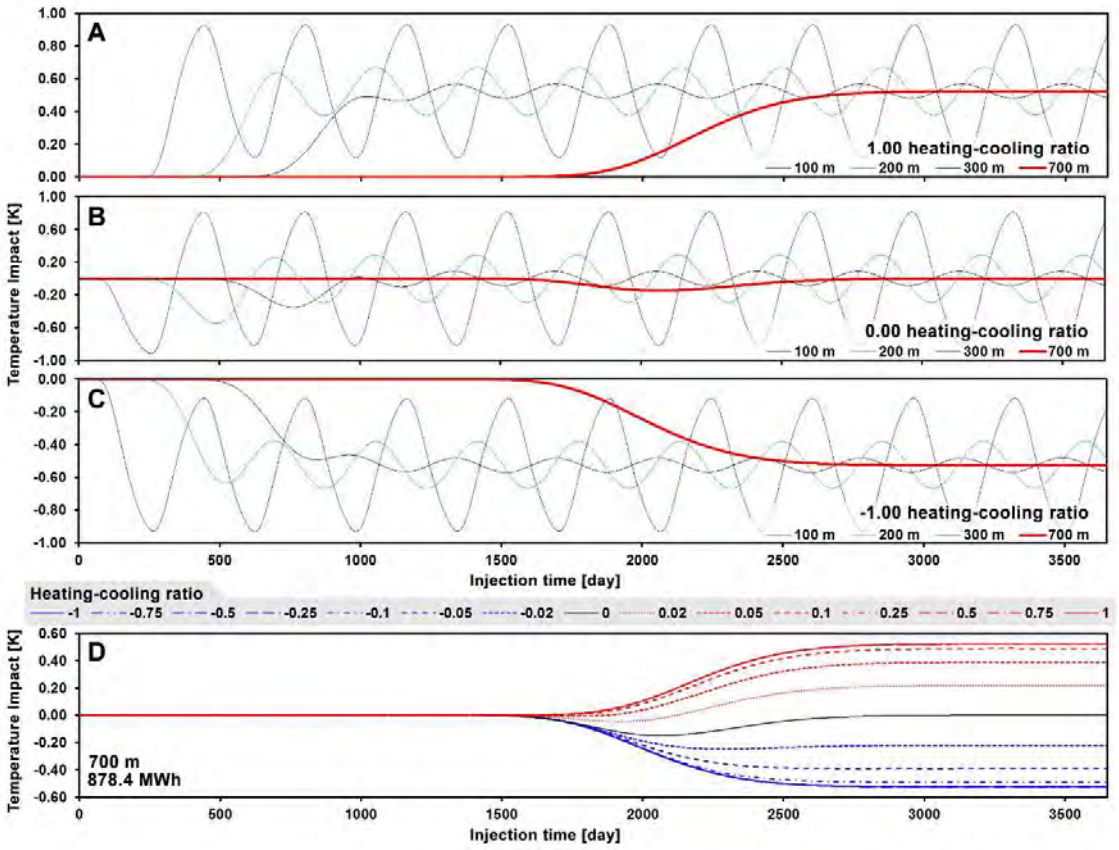

319

320 **Fig. 4.** Temporal distribution of thermal impacts at 100, 200, 300 and 700 m from the
321 injection point, 878.4 MWh maximum seasonal energy load and 1.00 (A), 0.00 (B) and -
322 1.00 (C) heating-cooling ratios. Temporal distribution of thermal impacts at 700 m from
323 the injection point, 878.4 MWh maximum seasonal energy load and all evaluated heating-
324 cooling ratios is also shown (D).

325

326 The non-oscillatory thermal impact associated to the 75 heating-cooling scenarios proposed
327 in this work is shown in Fig. 5A as a function of HC ratios and maximum seasonal energy
328 loads. It should be mentioned that the non-oscillatory thermal impact increases

329 exponentially with the maximum seasonal energy loads (Fig. 5A). The non-oscillatory
330 thermal impact is almost independent of the HC ratio in the range of ±0.10 to ±1.00. In
331 contrast, in the 0 to ±0.10 range (Fig. 5C), there is a clear thermal impact reduction (as seen
332 in figures 4 and 5) up to 3 orders of magnitude. The symmetry of the non-oscillatory
333 thermal impact with respect to the HC ratio allows to consider absolute ratios hereafter. The
334 sign of the thermal impacts could be directly deduced by comparing heating load and
335 thermal load.

336

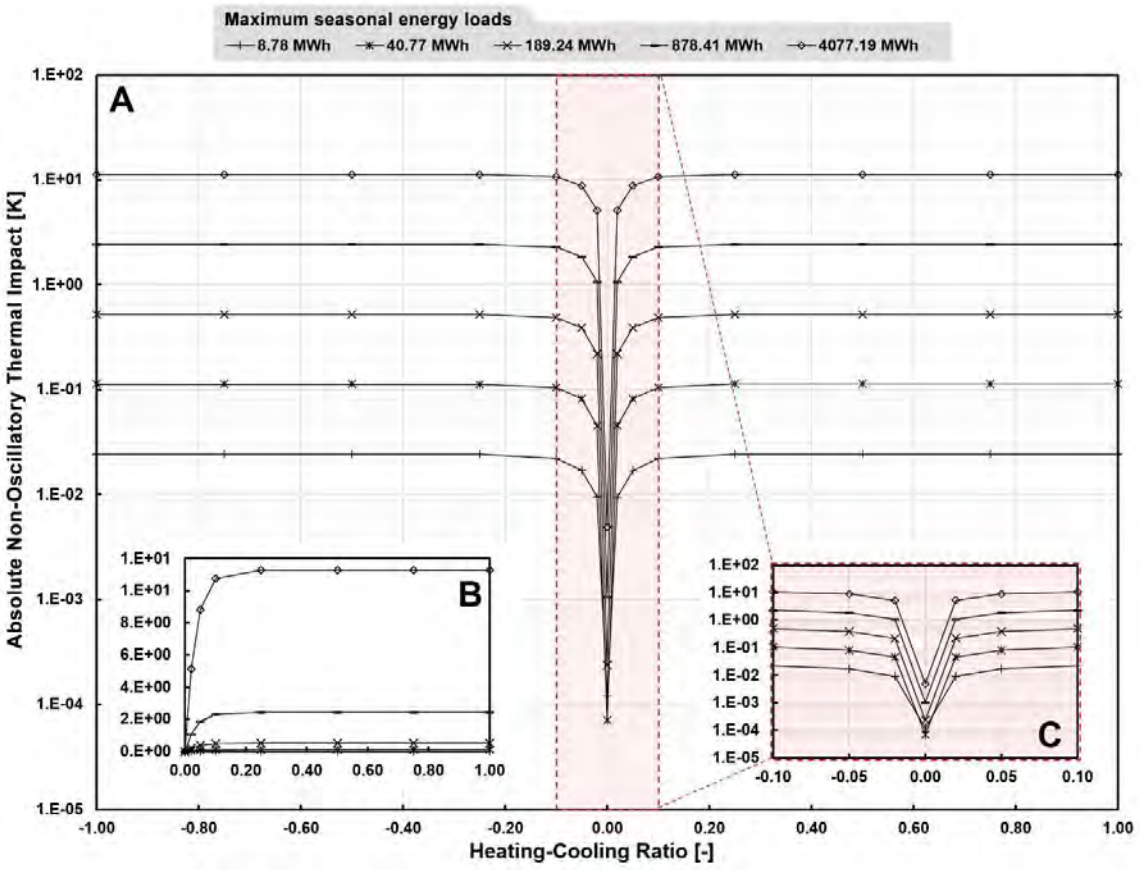

337

338 **Fig. 5.** Absolute non-oscillatory thermal impact associated to the heating-cooling scenarios
339 for the different maximum seasonal energy loads at a logarithmic scale (A) and non-

logarithmic scale (B). Detailed absolute non-oscillatory thermal impact in the 0 to ±0.10 range is shown (C). Negative values of the heating-cooling represent heating loads greater than cooling, and vice versa.

3.2 BSI calculation and validation results

The non-oscillatory thermal impacts were assumed to describe the sustainability of a GWHP and the value of this variable is directly used as the BSI indicator. The regression analysis performed allowed to obtain two polynomial regression models provided in Table II to calculate directly BSI from the HC ratio and the maximum seasonal energy load of any GWHP system. Since an unique polynomial regression model was not able to fit the whole 75 scenario dataset, two models were calculated: a polynomial regression model 1 for the 0.00 to 0.10 HC ratio range (Fig. 6A) and a second polynomial regression model 2 for a HC ratio equal or greater than 0.10 (Fig. 6B). The goodness of fit is supported by a RMSE of 7.52E-4 and 1.72E-2 K for model 1 and 2, respectively. The validation of the polynomial regression models against 23 real GWHP systems showed an error below 8% in all cases, and below 2% in 87% of the data validated. The error is mainly generated by GWHP systems with a HC ratio larger than 0.10. This is explained by the polynomial regression model 2 with the lowest RMSE. The largest error is derived from G-19, which presents a very low HC ratio, close to the balanced regime of operation and the lowest maximum seasonal thermal load. This indicates that the accuracy of the polynomial models proposed is compromised for GWHP systems operating below 1.43E+01 MWh as the maximum seasonal thermal load, which are the smallest systems. Further analysis on validation results are provided as Supplementary material (S2).

363

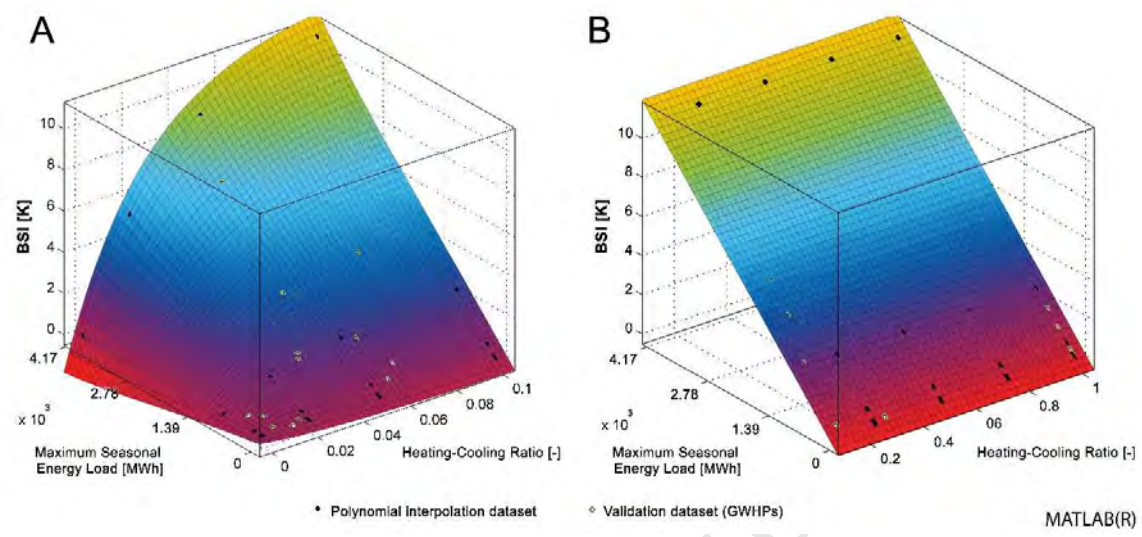

364

365 **Fig. 6.** Plots of polynomial regression model 1(A) and 2(B) obtained from the interpolation
366 of non-oscillatory thermal impacts of the 75 heating-cooling scenarios considered. Non-
367 oscillatory thermal impacts of the real GWHP systems used for validation are also shown.

368

369

370

Polynomial regression model 1

$f(x,y) = p00 + p10x + p01y + p20x^2 + p11xy + p02y^2 + p30x^3 + p21x^2y + p12xy^2 + p03y^3 + p40x^4 + p31x^3y + p22x^2y^2 + p13xy^3 + p04y^4 + p50x^5 + p41x^4y + p32x^3y^2 + p23x^2y^3 + p14xy^4 + p05y^5$

Coefficients	
p00	2.814E-04
p10	-3.698E-01
p01	-9.965E-16
p20	1.917E+01
p11	2.126E-11
p02	9.720E-28
p30	-2.790E+02
p21	-2.888E-10
p12	2.652E-25
p03	-1.733E-40
p40	1.254E+02
p31	2.229E-09
p22	-3.606E-24
p13	-1.318E-38
p04	-5.020E-54
p50	1.108E+04
p41	-7.408E-09
p32	1.078E-23
p23	8.558E-38
p14	3.186E-52
p05	8.852E-67

*x = heating-cooling ratio [-]
*y = Maximum seasonal energy loads [J]

Polynomial regression model 2

$f(x,y) = p00 + p10x + p01y + p20x^2 + p11xy + p02y^2 + p30x^3 + p21x^2y + p12xy^2 + p03y^3 + p40x^4 + p31x^3y + p22x^2y^2 + p13xy^3 + p04y^4 + p50x^5 + p41x^4y + p32x^3y^2 + p23x^2y^3 + p14xy^4$

Coefficients	
p00	-7.132E-02
p10	1.283E+00
p01	6.548E-13
p20	-7.305E+00
p11	8.366E-13
p02	1.364E-26
p30	1.763E+01
p21	-2.172E-12
p12	-4.862E-26
p03	-1.360E-39
p40	-1.876E+01
p31	2.492E-12
p22	2.433E-26
p13	4.294E-39
p04	3.779E-53
p50	7.222E+00
p41	-1.039E-12
p32	7.420E-27
p23	-2.195E-39
p14	-7.063E-53

*x = heating-cooling ratio [-]
*y = Maximum seasonal energy loads [J]

Table II. Polynomial regression model 1(A) and 2(B) obtained from the interpolation of non-oscillatory thermal impacts of the 75 heating of non-oscillatory thermal impacts of the 75 heating-cooling scenarios considered. Maximum seasonal thermal load were considered in joules

3.3 The BSI indicator in shallow geothermal resources management and its limitations

When city managers face the authorization and surveillance of GWHP systems, whether already existing or expected to operate in the future, they need scientifically-based criteria to ensure sustainability of their city subsurface energy resources' exploitation. The BSI indicator provides a first general view of the potential sustainability of the operating systems. The BSI indicator applied to the GWHP systems of the city of Zaragoza is shown in Fig. 7. This indicator clearly evidences the different situations in terms of potential sustainability. G-1 installation is by far the most potentially unsustainable. This installation would potentially produce, in the standard model of reference proposed, a non-oscillatory

386 thermal impact of 11 K 700 m downgradient. This is not a prediction for the real world
387 since all hydraulic and thermal parameters considered in the standard numerical model are
388 different to those found in each specific real world case. Furthermore, the heating and
389 cooling loads were distributed constantly over 6 months, which is not necessarily the
390 general case. This is a clear limitation of the method. The BSI indicator is not as accurate as
391 if each GWHP system would have a calibrated and validated numerical model associated
392 incorporating all hydrogeological settings and specific operation regimes. However, this
393 limitation can be easily overcome if these realistic numerical models are available to the
394 manager. The BSI indicator could be calculated following the procedure provided in this
395 work, replacing the "standard numerical model of reference" by the specifically adapted
396 one to the local conditions. In this case, the BSI indicator should be named BSIA, i.e.,
397 "*adapted BSI*". This specific term is required since those indicators would be not
398 comparable worldwide in other urban areas. BSIA would be more reliable for city
399 managers, but they would be no longer normalized by the "standard numerical model of
400 reference" proposed in this work.

401

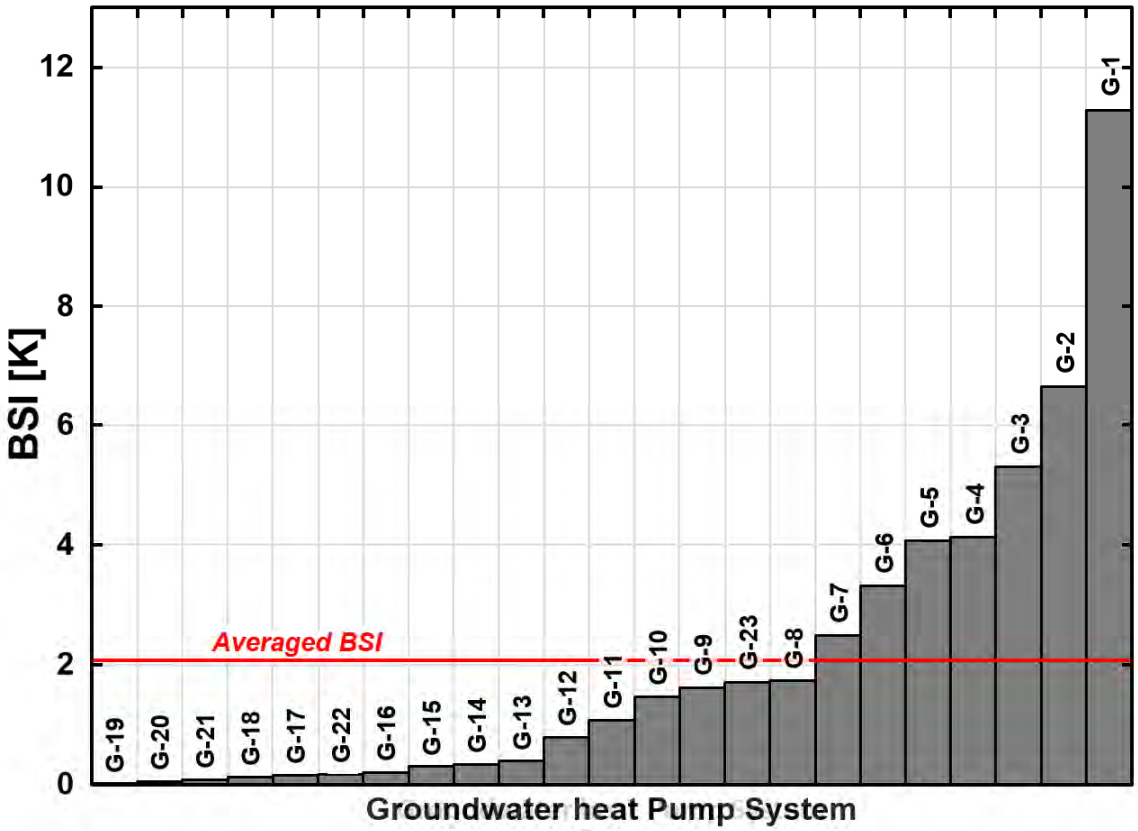

402

403 **Fig. 7.** BSI indicator applied to the 23 GWHP systems of city of Zaragoza [32].

404

405 Nevertheless, the BSI indicator does provide a reference framework for hydrogeologists
406 and technicians as a normalized view of the GWHP systems in operation, which is of
407 importance in order to design geothermal monitoring networks or prioritize specific local
408 studies investigating the potential thermal interferences between systems. The BSI indicator
409 can also be calculated for yet to be constructed GWHP systems, thus providing city
410 managers with an idea of the appropriateness of emplacing a given projected installation in
411 a given area. In the case study provided, G-1 system should be considered for control, by
412 means of installation monitoring or downgradient monitoring by the construction of a

piezometer if aquifer monitoring is planned, especially if there are GWHP systems downgradient. The same treatment should be considered for G-2, G-3, G-4, G-5, G-6 and G-7, establishing a priority proportional to magnitude of the BSI indicator. On the other hand, G-19, G-20, G-21, G-18, G-17, G-22, G-16, G-15, G-14 and G-13 are relatively well-balanced installations. In addition, when a group of installations present similar BSI indicators, the HC ratio could be additionally considered (Table I). E.g., G-22 presents a larger maximum thermal load than that of G-22, but the latter has a smaller BSI, due to G-22 having a lower HC ratio, i.e., G-22 installation is better thermally-balanced. Therefore, G-22 is potentially using more efficiently the city shallow geothermal energy resources. These examples demonstrate the usefulness of the BSI indicator as an objective tool to reinforce effective and sustainable installations. Nevertheless, this indicator needs to be complemented with other indicators relative to real thermal impacts produced in the groundwater body managed to verify the possible risk of thermal interferences and other possible conflicts. The IRF indicator [36] showing the real accumulated thermal impacts in pumping wells of GWHP systems and the piezometers from geothermal monitoring networks, combined with the BSI indicator proposed would complete the cause-effect relationship between the GWHPs systems and the urban subsurface environment. Moreover, if a downgradient installation's IRF (IRF_{down}) is compared to the corresponding upgradient installation's BSI (BSI_{up}), this could provide a *Thermal Interference Sustainability* (TIS) indicator between installations, given by the following expression:

$$TIS = BSI_{up} \cdot IRF_{down} \quad (1)$$

435 The greater the thermal interference generated (greater IRF_{down}) by an unsustainable
436 GWHP system (greater BSI_{up}), the more unsustainable this situation would be and the
437 more attention it would need from city managers. Other application of the BSI indicator is
438 comparing GWHP systems between different case studies or assigning a mean BSI for the
439 city considered. For the urban aquifer of Zaragoza, this mean BSI would be 2.07 K (Fig. 7).
440 Moreover, this indicator could be updated every year to monitor the evolution of the
441 systems and to validate the efficiency of the actions taken against the unsustainable use of
442 shallow geothermal resources such as financial incentives or other support tools/flanking
443 measures to boost the development of these renewable technologies [2].Finally, it is to be
444 highlighted that the BSI indicator is not an end-solution to shallow geothermal resources
445 management in cities. It provides an objective criteria to establish/design geothermal
446 monitoring programs to control thermal impacts and to develop city-scale numerical
447 groundwater and heat transport models [30, 31] that would finally provide city managers
448 with the real thermal state of the aquifer [46] and possible exploitation-remediation
449 scenarios [32, 35].

4 Conclusions

The present investigation has proposed a novel indicator for city managers to face the characterization of managed GWHP systems in terms of potential intrinsic sustainability. After the definition of the indicator and the discussion of its applicability and limitations, the following conclusions can be highlighted: (1) The BSI indicator provides a first general view of the potential sustainability of the operating systems from a quantitative perspective by making use of simple installation operational parameters. (2) The indicator provides a reference framework for hydrogeologists and technicians in order to harmonize thermal impacts of GWHP systems. This allows comparing intrinsic potential sustainability of these systems independently of the hydrogeological conditions worldwide. Therefore, the indicator has no capability to predict real thermal impacts of a GWHP. However, it does provide the standardized thermal impact under normalized conditions without performing any numerical modelling. (3) The validation of the polynomial regression models underpinning the BSI indicator showed an error below 8% for all the data validated, thus ensuring the accuracy of the BSI indicator for GWHP systems operating with maximum seasonal thermal load in the range of 1.43E+01 to 4.17E+03 MWh. (4) The BSI indicator applied to 23 real GWHP systems evidences its usefulness in the identification of different groups of installations that deserve different management policies to prevent plausible thermal interferences. (5) The design of geothermal monitoring networks could make use of the BSI indicator to focus control and prioritize specific areas where potential unsustainable systems are located. This would target monitoring efforts to efficiently prevent thermal interference between systems.

Finally, this indicator is not an end-solution to shallow geothermal energy management of urban groundwater bodies. It can be considered as a first step in the roadmap of establishing city-scale management policies for shallow geothermal energy. The potential intrinsic sustainability evaluation of a GWHP system using the BSI indicator could provide the administrators with an objective tool to design geothermal monitoring programs required to develop complex decision-support models based on numerical modeling. Further developments of the BSI indicator include its complementation with other indicators relative to real thermal impacts produced in the aquifer managed to verify the possible risk of thermal interferences and other possible conflicts.

5. Acknowledgments

This work was performed by the Geological Survey of Spain (IGME) under the Cooperation Agreement framework between IGME and the Ebro Hydrographic Confederation (CHE) for the specific arrangement entitled “The application of a groundwater flow and heat transport numerical model for the simulation of management strategies of geothermal installations in the city of Zaragoza”. Alejandro García-Gil gratefully acknowledges MIKE by DHI for the sponsored FEFLOW license.

7 References

[1] B. Sanner, L. Angelino, M. De Gregorio, N. Février, W. Haslinger, A. Kujbus, S. Landolina, W. Sparber, G. Stryi-Hipp, W. van Helden, W. Weiss, Strategic Research and Innovation Agenda for Renewable Heating & Cooling, RHC-Platform, Brussels, 2013.

[2] F. Jaudin, D2.2: General Report of the current situation of the regulative framework for the SGE systems, REGEOCITIES, 2013, p. 50.

[3] J.W. Lund, T.L. Boyd, Direct Utilization of Geothermal Energy 2015 Worldwide Review, World Geothermal Congress 2015, Melbourne, Australia, 2015, p. 31.

[4] O. Edenhofer, R. Pichs Madruga, Y. Sokona, Renewable energy sources and climate change mitigation: summary for policymakers and technical summary—special report of the intergovernmental panel on climate change, New York, 2012.
[5] J.W. Lund, T.L. Boyd, Direct utilization of geothermal energy 2015 worldwide review, Geothermics 60(Supplement C) (2016) 66-93.
[6] L. Rybach, The advance of geothermal heat pumps world-wide., International Energy Agency (IEA) Heat Pump Centre Newsletter 2005, 2005, pp. 13–18.
[7] L. Junghans, Evaluation of the economic and environmental feasibility of heat pump systems in residential buildings, with varying qualities of the building envelope, Renewable Energy 76 (2015) 699-705.
[8] M.L. Dû, Y. Dutil, D.R. Rousse, P.L. Paradis, D. Groulx, Economic and energy analysis of domestic ground source heat pump systems in four Canadian cities, Journal of Renewable and Sustainable Energy 7(5) (2015) 053113.
[9] R. DiPippo, J.L. Renner, Chapter 22 - Geothermal Energy, in: T.M. Letcher (Ed.), Future Energy (Second Edition), Elsevier, Boston, 2014, pp. 471-492.
[10] S.J. Self, B.V. Reddy, M.A. Rosen, Geothermal heat pump systems: Status review and comparison with other heating options, Applied Energy 101 (2013) 341-348.
[11] K. Rafferty, Capital cost comparison of commercial ground-source heat pump systems, in: A. Jelaic (Ed.) Proc. Geotherm. Prog. Rev. 14th, DOE, Washington, DC, 1995, pp. 261-265.
[12] J.W. Lund, Direct-use of geothermal energy in the USA, Applied Energy 74(1) (2003) 33-42.
[13] J.E. Mock, J.W. Tester, P.M. Wright, GEOTHERMAL ENERGY FROM THE EARTH:Its Potential Impact as an Environmentally Sustainable Resource, Annual Review of Energy and the Environment 22(1) (1997) 305-356.
[14] S. Lo Russo, L. Gnavi, E. Roccia, G. Taddia, V. Verda, Groundwater Heat Pump (GWHP) system modeling and Thermal Affected Zone (TAZ) prediction reliability: Influence of temporal variations in flow discharge and injection temperature, Geothermics 51 (2014) 103-112.
[15] J.W. Lund, D.H. Freeston, T.L. Boyd, Direct utilization of geothermal energy 2010 worldwide review, Geothermics 40(3) (2011) 159-180.
[16] S. Haehnlein, P. Bayer, P. Blum, International legal status of the use of shallow geothermal energy, Renewable and Sustainable Energy Reviews 14(9) (2010) 2611-2625.
[17] A. Galgaro, M. Cultrera, Thermal short circuit on groundwater heat pump, Applied Thermal Engineering 57(1-2) (2013) 107-115.
[18] J.A. Rivera, P. Blum, P. Bayer, Increased ground temperatures in urban areas: Estimation of the technical geothermal potential, Renewable Energy 103 (2017) 388-400.
[19] K. Zhu, P. Blum, G. Ferguson, K.D. Balke, P. Bayer, The geothermal potential of urban heat islands (vol 5, 044002, 2010), Environmental Research Letters 6(1) (2011).
[20] S.A. Benz, P. Bayer, K. Menberg, S. Jung, P. Blum, Spatial resolution of anthropogenic heat fluxes into urban aquifers, Science of the Total Environment 524–525(0) (2015) 427-439.
[21] NGWA, Geothermal Heating & Cooling Survey, National Ground Water Association, 2010.
[22] D. Banks, Thermogeological assessment of open-loop well-doublet schemes: a review and synthesis of analytical approaches, Hydrogeology Journal 17(5) (2009) 1149-1155.
[23] G. Rock, H. Kupfersberger, 3D modeling of groundwater heat transport in the shallow Westliches Leibnitzer Feld aquifer, Austria, Journal of Hydrology 557 (2018) 668-678.
[24] J. Epting, S. Scheidler, A. Affolter, P. Borer, M.H. Mueller, L. Egli, A. García-Gil, P. Huggenberger, The thermal impact of subsurface building structures on urban groundwater resources – A paradigmatic example, Science of the Total Environment 596-597 (2017) 87-96.
[25] G. Attard, T. Winiarski, Y. Rossier, L. Eisenlohr, Review: Impact of underground structures on the flow of urban groundwater, Hydrogeology Journal 24(1) (2016) 5-19.

[26] E. Vázquez-Suñé, X. Sánchez-Vila, J. Carrera, Introductory review of specific factors influencing urban groundwater, an emerging branch of hydrogeology, with reference to Barcelona, Spain, Hydrogeology Journal 13(3) (2005) 522-533.
[27] A. García-Gil, E. Vázquez-Suñe, E. Garrido, J.A. Sánchez-Navarro, J. Mateo-Lázaro, The thermal consequences of river-level variations in an urban groundwater body highly affected by groundwater heat pumps, Science of the Total Environment (2014).
[28] L.R.S. Baccino Giorgia, Taddia Glenda, Verda Vittorio, Energy and environmental analysis of an open-loop ground-water heat pump system in an urban area, Thermal Science 14(3) (2010) 13.
[29] G. Florides, S. Kalogirou, Ground heat exchangers—A review of systems, models and applications, Renewable Energy 32(15) (2007) 2461-2478.
[30] F. Händel, R. Liedl, J. Fank, G. Rock, Regional modeling of geothermal energy systems in shallow aquifers: the Leibnitzer Feld case study (Austria), Environ. Earth Sci. 70(8) (2013) 3433-3446.
[31] A. Herbert, S. Arthur, G. Chillingworth, Thermal modelling of large scale exploitation of ground source energy in urban aquifers as a resource management tool, Applied Energy 109(0) (2013) 94-103.
[32] A. García-Gil, E. Vázquez-Suñé, J.A. Sánchez-Navarro, J. Lázaro, Recovery of energetically overexploited urban aquifers using surface water, Journal of Hydrology 1(1) (2015) 111.
[33] J. Epting, A. García-Gil, P. Huggenberger, E. Vázquez-Suñe, M.H. Mueller, Development of concepts for the management of thermal resources in urban areas – Assessment of transferability from the Basel (Switzerland) and Zaragoza (Spain) case studies, Journal of Hydrology 548 (2017) 697-715.
[34] G. Attard, Y. Rossier, T. Winiarski, L. Eisenlohr, Deterministic modeling of the impact of underground structures on urban groundwater temperature, Science of the Total Environment 572 (2016) 986-994.
[35] J. Epting, F. Händel, P. Huggenberger, Thermal management of an unconsolidated shallow urban groundwater body, Hydrol. Earth Syst. Sci. 17(5) (2013) 1851-1869.
[36] A. García-Gil, E. Vázquez-Suñe, E.G. Schneider, J.Á. Sánchez-Navarro, J. Mateo-Lázaro, Relaxation factor for geothermal use development – Criteria for a more fair and sustainable geothermal use of shallow energy resources, Geothermics 56(0) (2015) 128-137.
[37] D. Katunsky, A. Korjenic, J. Katunska, M. Lopusniak, S. Korjenic, S. Doroudiani, Analysis of thermal energy demand and saving in industrial buildings: A case study in Slovakia, Building and Environment 67 (2013) 138-146.
[38] Y. Ding, Q. Zhang, T. Yuan, K. Yang, Model input selection for building heating load prediction: A case study for an office building in Tianjin, Energy and Buildings 159 (2018) 254-270.
[39] S. Lo Russo, M.V. Civita, Open-loop groundwater heat pumps development for large buildings: A case study, Geothermics 38(3) (2009) 335-345.
[40] A.D. Chiasson, Geothermal Heat Pump and Heat Engine Systems: Theory And Practice, Wiley2016.
[41] A. García-Gil, J. Epting, E. Garrido, E. Vázquez-Suñé, J.M. Lázaro, J.Á. Sánchez Navarro, P. Huggenberger, M.Á.M. Calvo, A city scale study on the effects of intensive groundwater heat pump systems on heavy metal contents in groundwater, Science of the Total Environment 572 (2016) 1047-1058.
[42] S. Muela Maya, A. García-Gil, E. Garrido Schneider, M. Mejías Moreno, J. Epting, E. Vázquez-Suñé, M.Á. Marazuela, J.Á. Sánchez-Navarro, An upscaling procedure for the optimal implementation of open-loop geothermal energy systems into hydrogeological models, Journal of Hydrology 563 (2018) 155-166.

592 [43] MathWorks, MATLAB and Statistics Toolbox Release 2012b, Natick, Massachusetts, United
593 States, 2012.
594 [44] E. Ostertagová, Modelling using Polynomial Regression, Procedia Engineering 48 (2012) 500-
595 506.
596 [45] H.J. Diersch, FEFLOW: Finite Element Modeling of Flow, Mass and Heat Transport in Porous
597 and Fractured Media, Springer Berlin Heidelberg2013.
598 [46] J. Epting, P. Huggenberger, Unraveling the heat island effect observed in urban groundwater
599 bodies – Definition of a potential natural state, Journal of Hydrology 501(0) (2013) 193-204.

600

601

602 **Figure and Table captions**

603 **Fig. 1.** Figure 1. 2D finite element mesh and boundary conditions used in the standard
604 numerical model used for the definition of the BSI index.

605 **Fig. 2.** Thermal energy loads of 23 groundwater heat pump systems from Zaragoza City
606 [32]. Theoretical thermal energy load scenarios simulated for different heating-cooling
607 ratios are also shown.

608 **Fig. 3.** Spatial distribution of thermal impacts calculated from the simulation of the 75
609 heating-cooling scenarios after 10 years of simulation. In the top of the figure, the relative
610 thermal impact is represented against distance in the *x* direction from the injection point
611 parallel to regional groundwater flow. The relative thermal impact is shown for different
612 heating-cooling ratios and a maximum seasonal energy load of 4077.19 MWh. In the
613 bottom, the heat plumes extension for a ±0.01 K increase for the different maximum
614 seasonal energy loads is shown. Negative values of the heating-cooling represent heating
615 loads greater than cooling, and vice versa.

616 **Fig. 4.** Temporal distribution of thermal impacts at 100, 200, 300 and 700 m from the
617 injection point, 878.4 MWh maximum seasonal energy load and 1.00 (A), 0.00 (B) and -

618 1.00 (C) heating-cooling ratios. Temporal distribution of thermal impacts at 700 m from
619 the injection point, 878.4 MWh maximum seasonal energy load and all evaluated heating-
620 cooling ratios is also shown (D).

621 **Fig. 5.** Absolute non-oscillatory thermal impact associated to the heating-cooling scenarios
622 for the different maximum seasonal energy loads at a logarithmic scale (A) and non-
623 logarithmic scale (B). Detailed absolute non-oscillatory thermal impact in the 0 to ±0.10
624 range is shown (C). Negative values of the heating-cooling represent heating loads greater
625 than cooling, and vice versa.

626 **Fig. 6.** Plots of polynomial regression model 1(A) and 2(B) obtained from the interpolation
627 of non-oscillatory thermal impacts of the 75 heating-cooling scenarios considered. Non-
628 oscillatory thermal impacts of the real GWHP systems used for validation are also shown.

629 **Fig. 7.** BSI indicator applied to the 23 GWHP systems of city of Zaragoza [32].

630 **Table I.** Thermal loads of the 23 GWHP system studied [32] and the parameters required to
631 calculate BSI index. Absolute errors obtained from validation process is also included.

632 **Table II.** Polynomial regression model 1(A) and 2(B) obtained from the interpolation of
633 non-oscillatory thermal impacts of the 75 heating of non-oscillatory thermal impacts of the
634 75 heating-cooling scenarios considered. Maximum seasonal thermal load were considered
635 in joules.

636

Groundwater heat pump system	Heating load [MWh]	Cooling load [MWh]	Maximum seasonal thermal load [MWh]	Heating-cooling ratio [-]	BSI simulated [K]	BSI calculated [K]	Error [%]
G-1	4.07E+03	9.34E-01	4.07E+03	0.276	11.276	11.452	1.563
G-2	3.25E+03	8.47E+02	3.25E+03	0.045	6.656	6.659	0.038
G-3	1.92E+03	1.15E+01	1.92E+03	0.173	5.297	5.296	0.011
G-4	1.69E+03	1.97E+02	1.69E+03	0.073	4.132	4.135	0.071
G-5	1.48E+03	1.21E+01	1.48E+03	0.164	4.070	4.068	0.052
G-6	1.71E+03	5.10E+02	1.71E+03	0.041	3.313	3.314	0.033
G-7	9.20E+02	2.11E+01	9.20E+02	0.131	2.489	2.488	0.026
G-8	7.90E+02	1.63E+02	7.90E+02	0.055	1.738	1.738	0.026
G-9	9.52E+02	3.67E+02	9.52E+02	0.033	1.621	1.622	0.021
G-10	8.76E+02	3.49E+02	8.76E+02	0.032	1.460	1.460	0.011
G-11	3.85E+02	0.00E+00	3.85E+02	1.000	1.067	1.051	1.468
G-12	3.46E+02	6.10E+01	3.46E+02	0.062	0.790	0.790	0.011
G-13	1.79E+02	3.79E+01	1.79E+02	0.057	0.390	0.391	0.259
G-14	1.28E+02	4.67E+00	1.28E+02	0.123	0.343	0.344	0.198
G-15	1.09E+02	0.00E+00	1.09E+02	1.000	0.301	0.299	0.553
G-16	3.75E+02	3.02E+02	3.75E+02	0.008	0.201	0.201	0.299
G-17	5.71E+01	0.00E+00	5.71E+01	1.000	0.158	0.157	0.683
G-18	4.39E+01	2.30E-02	4.39E+01	0.293	0.122	0.120	1.438
G-19	1.04E+01	1.43E+01	1.43E+01	0.013	0.011	0.010	7.898
G-20	9.93E+01	1.18E+02	1.18E+02	0.006	0.051	0.052	0.739
G-21	5.16E+01	8.06E+01	8.06E+01	0.017	0.080	0.081	1.674
G-22	4.73E+02	5.35E+02	5.35E+02	0.004	0.171	0.171	0.066
G-23	0.00E+00	6.18E+02	6.18E+02	1.000	1.712	1.673	2.283

Polynomial regression model 1

f(x,y) = p00 + **p10**x + **p01**y + **p20**x^2 + **p11**xy + **p02**y^2 + **p30**x^3 + **p21**x^2y
+ **p12**xy^2 + **p03**y^3 + **p40**x^4 + **p31**x^3y + **p22**x^2y^2
+ **p13**xy^3 + **p04**y^4 + **p50**x^5 + **p41**x^4y + **p32**x^3y^2
+ **p23**x^2y^3 + **p14**xy^4 + **p05**y^5

Coefficients

p00	2.814E-04
p10	-3.698E-01
p01	-9.965E-16
p20	1.917E+01
p11	2.126E-11
p02	9.720E-28
p30	-2.790E+02
p21	-2.888E-10
p12	2.652E-25
p03	-1.733E-40
p40	1.254E+02
p31	2.229E-09
p22	-3.606E-24
p13	-1.318E-38
p04	-5.020E-54
p50	1.108E+04
p41	-7.408E-09
p32	1.078E-23
p23	8.558E-38
p14	3.186E-52
p05	8.852E-67

x = heating-cooling ratio [-]

y = Maximum seasonal energy loads [J]

Polynomial regression model 2

f(x,y) = **p00** + p10x + p01y + p20x^2 + p11xy + p02y^2 + p30x^3 + p21x^2y + p12xy^2
+ p03y^3 + p40x^4 + p31x^3y + p22x^2y^2 + p13xy^3 + p04y^4 + p50x^5 + p41x^4y +
p32x^3y^2 + p23x^2y^3 + p14xy^4

Coefficients

p00	-7.132E-02
p10	1.283E+00
p01	6.548E-13
p20	-7.305E+00
p11	8.366E-13
p02	1.364E-26
p30	1.763E+01
p21	-2.172E-12
p12	-4.862E-26
p03	-1.360E-39
p40	-1.876E+01
p31	2.492E-12
p22	2.433E-26
p13	4.294E-39
p04	3.779E-53
p50	7.222E+00
p41	-1.039E-12
p32	7.420E-27
p23	-2.195E-39
p14	-7.063E-53

x = heating-cooling ratio [-]

y = Maximum seasonal energy loads [J]

Highlights

- An indicator for the management of open-loop geothermal systems is proposed
- Scientifically-based criteria to prevent thermal interferences are provided
- The indicator is applied to 23 groundwater heat pump systems